Dynamical stabilization of cubic ZrO_2 by phonon-phonon interactions: *Ab initio* calculations

P. Souvatzis and S. P. Rudin
Theoretical Division, Los Alamos National Laboratory, Los Alamos, New Mexico 87545, USA
(Received 30 September 2008; revised manuscript received 16 October 2008; published 11 November 2008)

Cubic zirconia exhibits a soft phonon mode (X_2^-) which becomes dynamically unstable at low temperatures. Previous *ab initio* investigations into the temperature-induced stabilization of the soft mode treated it as an independent anharmonic oscillator. Calculations presented here, using the self-consistent *ab initio* lattice-dynamical method to evaluate the phonons at 2570 K, show that the soft mode should not be treated independently of other phonon modes. Phonon-phonon interactions stabilize the X_2^- mode. Furthermore, the effective potential experienced by the mode takes on a quadratic form.

DOI: 10.1103/PhysRevB.78.184304 PACS number(s): 63.10.+a, 63.20.Ry

I. INTRODUCTION

Ab initio studies of the thermodynamics of solids rely heavily on the quasiharmonic approximation for describing the phonons.[1] The approximation treats the crystal lattice vibrations as harmonic at a sequence of volumes and, based on the frequencies usually calculated with the direct force method[2,3] or the linear-response method,[4] constructs, e.g., the free energy for each volume. The free energy can then be interpolated to describe the temperature- and volume-dependent thermodynamics. In numerous examples quasiharmonic theory has successfully predicted the low-temperature phonons[2,5–8] as well as thermal expansion, heat capacity, and thermal dependence of elastic properties.[3,9,10]

The success of quasiharmonic theory rests heavily on the absence of strong phonon-phonon interactions and of dynamical instabilities. Figure 1(a) illustrates a schematic potential-energy surface of a two-mode system in which both phonon-phonon interactions and dynamical instabilities are absent.

Some systems exhibit one or several dynamically unstable phonon modes, i.e., modes with imaginary harmonic frequencies.[11] Examples of such systems include the body-centered-cubic (bcc) phase of groups IIIB and IVB metals,[12] cubic zirconia,[13] and high-pressure bcc phase in Fe.[14,15] The unstable modes do not contradict experiments, which only observe these structures at high temperatures, where the quasiharmonic approximation cannot be applied. But the unstable modes do pose a problem for the theoretical evaluation of thermodynamic quantities.

Recent years have seen several attempts to deal with dynamical instabilities while retaining the convenience of keeping the phonon modes independent of one another,[16–18] a situation schematically illustrated in Fig. 1(b) by a two-mode system with one stable and one unstable mode. Assuming that the unstable phonon mode's (nonquadratic) potential remains independent of the other modes, these recent attempts approximate the potential as either a parabola combined with a Gaussian or as a quartic function, which leads to an analytical solution for the independent anharmonic oscillator. The solution provides a real frequency above a critical temperature T_c as well as the mode's contribution to the canonical partition function, which allows the evaluation of thermodynamic properties. The justification for this approach relies on the interactions between phonons remaining weak at temperatures up to the critical temperature.

Figure 1(c) illustrates a schematic potential-energy surface for a two-mode system in which the modes interact strongly and the independent anharmonic oscillator approximation cannot be justified. Here the simultaneous presence of different phonon modes creates geometric disorder, i.e., entropy which stabilizes the unstable mode.[19] Such entropy-driven stabilization has been studied, e.g., by Ye *et al.*,[20] who demonstrated by means of perturbation theory that the dynamical stabilization of the high-temperature bcc phase in Zr is the result of phonon-phonon interactions.

The work presented here investigates the role of phonon-phonon interactions in the high-temperature stabilization of cubic zirconia (ZrO_2) (space group $Fm3m$). Cubic zirconia shares several physical properties with diamond (although its use as a surrogate is not always appreciated) such as visual similarity, large hardness, and high melting temperature. In particular, neither cubic zirconia nor carbon in the diamond structure is a ground-state structure.

At ambient pressure, zirconia favors the cubic phase above temperatures of 2570 K. Below this temperature, the material favors the tetragonal structure (space group $P4_2/nmc$) down to 1400 K, below which a monoclinic phase emerges as most energetically favorable. At low tempera-

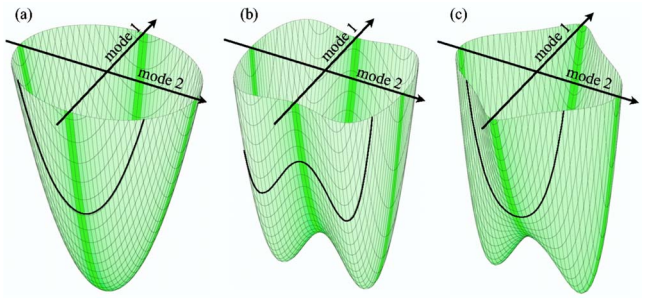

FIG. 1. (Color online) Schematic potential-energy surfaces for systems with two vibrational modes. The solid black curve illustrates the potential seen by the second mode for a fixed finite amplitude of the first mode. In (a), both modes are independent and stable. In (b), the second mode is unstable and independent of the first mode, i.e., always sees the same potential. In (c), the second mode is not independent of the first mode; for small amplitudes of the first mode, the second mode is unstable; for a large-enough amplitude of the first mode, the second mode becomes stable.

tures, ZrO_2 in the cubic phase is not only energetically unfavorable; it is also dynamically unstable.

The dynamic instability appears in the quasiharmonic approximation as imaginary frequency for the X_2^- phonon mode.[13,21,22] Previous studies[13,22] treat this unstable phonon mode as independent from other modes, i.e., neglect the effect of other phonon modes. The work presented here shows that the high-temperature dynamics of the X_2^- mode strongly depends on phonon-phonon interactions. Not only do other phonons stabilize the X_2^- phonon mode, but they make the potential it experiences at high temperatures quadratic.

II. DETAILS OF THE CALCULATIONS

The recently developed self-consistent *ab initio* lattice-dynamical (SCAILD) method[23,24] serves as a framework for the present study. The approach simulates a crystal with all phonon modes present simultaneously and thereby includes the interactions between them. The SCAILD method resembles the frozen-phonon method[25] in the use of supercells with atoms displaced according to the phonon mode eigenvectors. However, the two methods differ in four significant points:

(1) The frozen-phonon method displaces the atoms according to only one single phonon at a time, whereas the SCAILD method displaces the atoms simultaneously based on all phonons with wave vectors $\mathbf{k}$ found to be commensurate with the supercell. The presence of all phonons introduces geometric disorder, i.e., entropy, which in turn affects the phonon frequencies.

(2) The frozen-phonon method extracts each phonon mode's frequency from the dependence of the total energy on the mode's amplitude, whereas the SCAILD method obtains the frequencies based on the calculated Hellman-Feynman forces by projecting out each mode's restoring force.

(3) The frozen-phonon method evaluates each frequency once, whereas the SCAILD method relies on an iterative scheme to obtain a self-consistent phonon spectrum.

(4) In the frozen-phonon method the amplitudes of the atomic displacements are chosen by hand, whereas in the SCAILD method the amplitudes depend on temperature and the phonon frequencies.

Thermodynamics dictates at a given temperature T the population of each phonon mode s and accordingly the mode's amplitude $\mathcal{A}_{\mathbf{k}s}^{\sigma}$ based on the mode's frequency $\omega_{\mathbf{k}s}$; i.e.,

$$\mathcal{A}_{\mathbf{k}s}^{\sigma} = \pm \sqrt{\frac{\langle \mathcal{D}_{\mathbf{k}s}^{\sigma} \mathcal{D}_{-\mathbf{k}s}^{\sigma} \rangle}{M_{\sigma}}} = \pm \sqrt{\frac{\hbar}{M_{\sigma}\omega_{\mathbf{k}s}} \left[\frac{1}{2} + n\left(\frac{\hbar\omega_{\mathbf{k}s}}{k_B T} \right) \right]}, \tag{1}$$

where $n(x)=1/(e^x-1)$, M_{σ} denotes the mass of atoms of type σ, and $\mathcal{D}_{\mathbf{k}s}^{\sigma}$ represent the canonic phonon operators. These operators appear together with those for the canonical phonon momentum $\mathcal{P}_{\mathbf{k}s}^{\sigma}$ in the harmonic Hamiltonian $\mathcal{H}_h = \Sigma_{\mathbf{k},s,\sigma} \frac{1}{2} (\mathcal{P}_{\mathbf{k}s}^{\sigma} \mathcal{P}_{-\mathbf{k}s}^{\sigma} + \omega_{\mathbf{k}s}^2 \mathcal{D}_{\mathbf{k}s}^{\sigma} \mathcal{D}_{-\mathbf{k}s}^{\sigma})$.

As mentioned above, the SCAILD method excites all the phonons with wave vectors $\mathbf{k}$ commensurate with the supercell. In the supercell the undistorted atoms sit at $\mathbf{R}+\mathbf{b}_{\sigma}$, where $\mathbf{R}$ represent the N Bravais lattice sites of the supercell and $\mathbf{b}_{\sigma}$ is the position of atom σ relative to this site. The excitation of phonons displaces the atoms, $\mathbf{R}+\mathbf{b}_{\sigma} \rightarrow \mathbf{R}+\mathbf{b}_{\sigma}+\mathbf{U}_{\mathbf{R}\sigma}$, where

$$\mathbf{U}_{\mathbf{R}\sigma} = \frac{1}{\sqrt{N}} \sum_{\mathbf{k},s} \mathcal{A}_{\mathbf{k}s}^{\sigma} \epsilon_{\mathbf{k}s}^{\sigma} e^{i\mathbf{k}(\mathbf{R}+\mathbf{b}_{\sigma})}. \tag{2}$$

$\epsilon_{\mathbf{k}s}^{\sigma}$ are the eigenvectors of the dynamical matrix. The dynamical matrix for each wave vector arises from the Fourier transformation of the force-constant matrices $\bar{\bar{\Phi}}^{\sigma\sigma'}(\boldsymbol{R})$,

$$\mathcal{D}^{\sigma\sigma'}(\mathbf{k}) = \frac{1}{\sqrt{M_{\sigma} M_{\sigma'}}} \sum_{\boldsymbol{R}} \bar{\bar{\Phi}}^{\sigma\sigma'}(\boldsymbol{R}) e^{-i\mathbf{k}(\mathbf{R}+\mathbf{b}_{\sigma}-\mathbf{b}_{\sigma'})} \tag{3}$$

and satisfies the relation

$$\sum_{\sigma'} \mathcal{D}^{\sigma\sigma'}(\mathbf{k}) \epsilon_{\mathbf{k}s}^{\sigma'} = \omega_{\mathbf{k}s}^2 \sum_{\sigma} \epsilon_{\mathbf{k}s}^{\sigma}. \tag{4}$$

The SCAILD method alternates between displacing the atoms based on phonon frequencies and evaluating the phonon frequencies from *ab initio* calculated forces acting on the displaced atoms. For the first iterative step, the forces stem from a direct force method calculation (see, e.g., Refs. 2 and 3). The phonon frequencies and eigenvectors corresponding to commensurate $\mathbf{k}$ vectors are used to calculate a set of atomic displacements $\mathbf{U}_{\mathbf{R}}$ through Eqs. (1) and (2). A first-principles calculation provides the Hellman-Feynman forces acting on the displaced atoms, and new phonon frequencies are obtained from the Fourier transform $\mathbf{F}_{\mathbf{k}}^{\sigma}$ of the forces

$$\bar{\omega}_{\mathbf{k}s} = \left[\sum_{\sigma} \frac{\epsilon_{\mathbf{k}s}^{\sigma} \cdot \mathbf{F}_{\mathbf{k}}^{\sigma}}{\mathcal{A}_{\mathbf{k}s}^{\sigma} M_{\sigma}} \right]^{1/2}. \tag{5}$$

In order to make the sampling of the phonon frequencies more efficient, the symmetries of the different $\mathbf{k}$ vectors are restored for each iteration i by

$$\Omega_{\mathbf{k}s}^2(i) = \frac{1}{m_{\mathbf{k}}} \sum_{\mathcal{S} \in \mathcal{S}(\mathbf{k})} \bar{\omega}_{\mathcal{S}^{-1}\mathbf{k}s}^2(i), \tag{6}$$

where $\mathcal{S}(\mathbf{k})$ is the symmetry group of the wave vector $\mathbf{k}$ and m_k is the number of elements of the group. The symmetry-restored frequencies $\Omega_{\mathbf{k}s}(i), i=1,\ldots,N_I$ of all previous iterations provide a new set of frequencies $\omega_{\mathbf{k}s}^2(N_I)$

$$\omega_{\mathbf{k}s}^2(N_I) = \frac{1}{N_I} \sum_{i=1}^{N_I} \Omega_{\mathbf{k}s}^2(i), \tag{7}$$

which lead to a new set of atomic displacements $\mathbf{U}_{\mathbf{R}\sigma}$ through Eqs. (1) and (2), which in turn serve to calculate a new set of forces. Additional details of the method can be found in Refs. 23 and 24.

The forces are calculated using the VASP package.[26] Applying the local-density approximation (LDA), the exchange-correlation energy was evaluated with the Perdew-Wang parametrization[27] of Ceperly-Alder electron-gas data.[28] The projector-augmented wave (PAW) potentials used energy cutoffs of 480 eV. The $Zr(4s,4p,4d,5s)$ and $O(2s,2p)$ levels were treated as valence electrons. All calculations used the

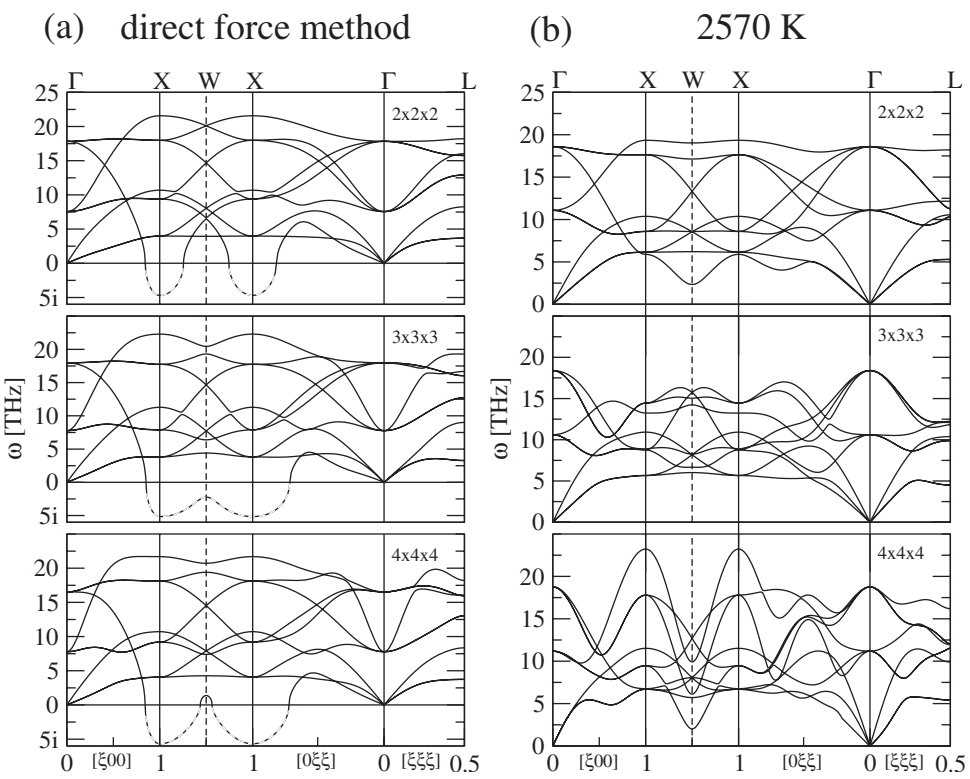

FIG. 2. The phonon dispersion of cubic ZrO_2 calculated with a 24-atom supercell (top row), an 81-atom supercell (middle row), and a 192-atom supercell (bottom row). The solid (and dashed) lines represent the first-principles phonon calculations. The left column (a) shows the results from the direct force method calculations (with the negative axis convention used for imaginary frequencies); the right column (b) shows the finite-temperature SCAILD calculations. The dashed lines on the left-hand side of the figure indicate imaginary phonon frequencies obtained in the direct force method calculations. At 2570 K these modes become stable, i.e., real, by including interaction between the phonons.

experimental lattice constant $a=5.09$ Å.[29] The effects of supercell size were investigated with simulation cells containing 24 atoms ($2\times2\times2$ supercell), 81 atoms ($3\times3\times3$ supercell), and 192 atoms ($4\times4\times4$ supercell). Convergence with respect to electronic **k** points required Monkhorst-Pack **k**-point grids of $7\times7\times7$ (for the 24-atom supercell), $6\times6\times6$ (for the 81-atom supercell), and $5\times5\times5$ (for the 192-atom supercell).

Born effective charges[30,31] were not used in the calculations presented in this paper. Therefore, no splitting between the optical longitudinal and optical transverse modes (LO/TO splitting) was obtained.

III. RESULTS

Figure 2 shows the results of the finite temperature SCAILD calculations for the cubic structure of ZrO_2 together with the results obtained with the direct force method calculations. For all supercell sizes, the direct force method calculations exhibit the same dynamical instability at the X [$\mathbf{k}=\frac{2\pi}{a}(1,0,0)$] high-symmetry point. This lattice instability of the longitudinal X_2^- phonon mode corresponds to the movement of the oxygen atoms along the direction of the phonon eigenvectors $\mathbf{e}_{\mathbf{k}s}^{\sigma}=(1,0,0)$. Figure 3 depicts the atomic displacements corresponding to the X_2^- phonon mode.

The right column of Fig. 2 shows the phonon dispersions resulting from the finite-temperature SCAILD calculations. Most importantly, the X_2^- phonon mode becomes stable and independent of supercell size. The frequency of the X_2^- phonon mode takes on the values of 5.89 (24 atoms), 8.78 (81 atoms), and 6.68 THz (192 atoms), which suggests a strong dependence on supercell size.

The convergence of numerical values for the frequencies with respect to supercell size cannot be established for the

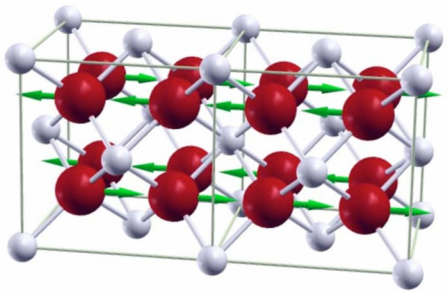

FIG. 3. (Color online) Schematic figure of the atomic movements corresponding to the soft longitudinal X_2^--point phonon mode of cubic ZrO_2. Here two unit cells of ZrO_2 are depicted with large red spheres representing oxygen atoms and small white spheres representing zirconium atoms. The green arrows, here pointing parallel to the [100] direction of the crystal, indicate the directions of the displacement of the oxygen atoms corresponding to the X_2^- phonon mode. (The Zr atoms are not displaced by this mode.)

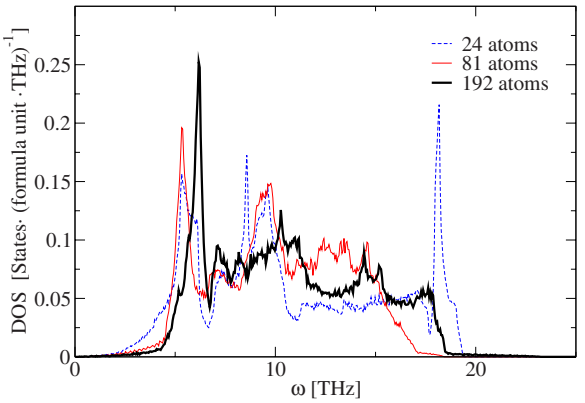

FIG. 4. (Color online) Phonon density of states for cubic ZrO_2 calculated with the SCAILD method. The dashed blue curve corresponds to the 24-atom supercell calculation, the thin red curve to the 81-atom supercell calculation, and the thick black curve to the 192-atom supercell calculation.

192-atom calculation. As in the direct force method calculation, the SCAILD method only evaluates the actual frequencies for phonon modes with commensurate wave vectors and interpolates the remaining frequencies plotted in the dispersions, which imparts some of the dependence on supercell size. The additional sensitivity to supercell size for the SCAILD calculations stems from the addition of phonon-phonon interactions, which depend on the phonon modes actually present in the supercell, i.e., only those with commensurate wave vectors contribute to the phonon-phonon interaction. Especially for small supercell sizes this implies that an increase in supercell size strongly influences the number of modes with which each phonon can interact. This sensitivity appears in the calculated values of the X_2^- phonon mode; these frequencies differ least between the 24-atom and 192-atom calculations because these supercells also share more commensurate wave vectors. The large discrepancy at the W high-symmetry point appears because the W point $(\frac{1}{2},\frac{1}{4},\frac{3}{4})$ is not a part of the commensurate $\mathbf{k}$-point set in the 24-atom calculation.

The sensitivity to supercell size also appears in the calculated phonon density of states (DOS) shown in Fig. 4 for the three supercell sizes. Although the commensurate wave vectors of the 24-atom supercell also appear in the 192-atom supercell, the two DOSs show striking differences. The DOS of the 24-atom calculation is considerably broader and it also exhibits a peak at high frequencies that disappears in the DOS of the 192-atom calculation. Larger supercells, needed to establish convergence of the phonon spectrum, currently exceed available computational resources. The sensitivity to supercell size impedes convergence of the frequencies' numerical values, but it compellingly suggests that the stabilization of the X_2^- phonon mode stems from strong phonon-phonon interactions; i.e., it cannot be treated independently from other phonon modes.

The effects of the other phonon modes stabilizing the X_2^- phonon mode can be seen by contrasting the effective potential experienced by X_2^- phonon mode at low and high temperatures. Figure 5(a) shows the frozen phonon, i.e., low-temperature potential-energy curve of the soft mode. The

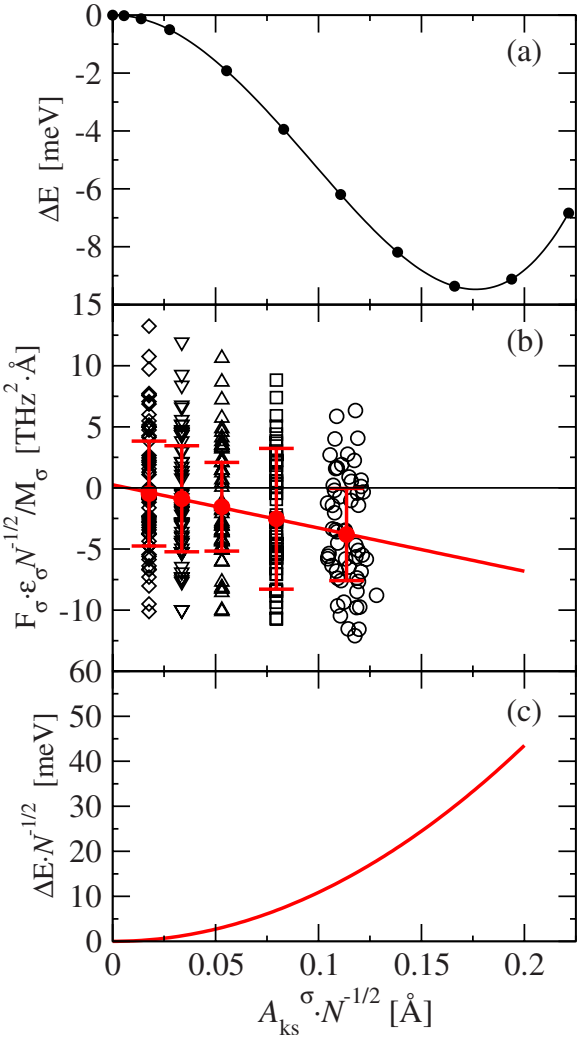

FIG. 5. (Color online) Calculated potential experienced by cubic zirconia's X_2^- phonon mode as a function of oxygen atom displacement in the independent phonon approximation and at 2570 K. (a) The calculated potential-energy curve has a local maximum at $\mathcal{A}_{\mathbf{ks}}^{\sigma}/\sqrt{N}=0$, reflecting cubic zirconia's lack of stability at low temperatures. (b) The calculated projected force in 24-atom supercells acting on the X_2^- phonon mode at 2570 K reflects cubic zirconia's stability at high temperatures. Empty symbols represent results evaluated for amplitudes either determined by Eq. (1) (empty circles) or fixed at values evident from the figure (empty diamonds, triangles, and squares). Filled red circles denote the geometrical mean values of the projected forces from each of the five sets of calculations, and the width of the error bars are two times the square root of the mean-square deviation of the projected forces relative to the geometrical mean values. The red dashed line plots a linear fit $F_p(\mathcal{A}_{\mathbf{ks}}^{\sigma}/\sqrt{N})$ of the mean values of the projected forces with $\alpha=-\frac{1}{2}\frac{dF_p(x)}{dx}=17.7$ THz^2. (c) Based on the linear fit, the phonon mode experiences an effective potential-energy curve $\Delta E = M_\sigma \alpha (\mathcal{A}_{\mathbf{ks}}^{\sigma}/\sqrt{N})^2$ at 2570 K that is quadratic.

dynamical instability of the ZrO_2 cubic phase is reflected in that the cubic structure sits at a local energy maximum.

Figure 5(b) shows the projections $\Sigma_\sigma \mathbf{F}_{\mathbf{k}}^{\sigma}\epsilon_{\mathbf{k}}^{\sigma}$ of the Fourier-transformed forces (taken from the iterations of the 2750 K calculation in the 24-atom supercell) plotted against the dis-

placement of the oxygen atoms, i.e., against the amplitude of the phonon mode given by Eq. (1). Also shown are the projected forces for SCAILD calculations with the X_2^- phonon mode's amplitude restricted to four specific numerical values (0.05, 0.095, 0.15, and 0.225 Å); all other phonon modes followed the SCAILD scheme outlined above. The resulting geometrical mean values of each of the five sets of iterations deviate by roughly 4.3% from a linear fit

$$\frac{1}{M}\left\langle \sum_{\sigma} \mathbf{F}_{\mathbf{k}}^{\sigma} \epsilon_{\mathbf{k}}^{\sigma} \right\rangle = 2\alpha \mathcal{A}_{\mathbf{k}s}^{\sigma} \tag{8}$$

with $\alpha = 17.7$ THz^2. The angular brackets $\langle\ \rangle$ denote the geometrical mean value. The approximately linear relationship between the restoring force and the amplitude suggests that phonon-phonon interactions stabilize the X_2^- phonon mode around 2570 K by making its effective potential quadratic.

Figure 5(c) shows the potential calculated from the linear relation (8). The phonon frequency obtained from the curvature of the resulting energy parabola, $\omega_{\mathbf{k}s} = \sqrt{2\alpha} = 5.95$ THz, is consistent with the frequencies 5.89, 8.78, and 6.68 THz obtained for the X_2^- phonon mode by the respective unrestricted 24-atom, 81-atom, and 192-atom calculations.

Based on the small height of the energy barrier in the potential-energy curve in Fig. 5(a), the X_2^- phonon mode could sample both sides of the temperature-independent potential-energy curve equally, i.e., it might "stabilize itself" without interacting with other phonons. This would result in amplitudes $\mathcal{A}_{\mathbf{k}s}^{\sigma} \gtrsim 0.18$ Å. However, achieving such amplitudes from Eq. (1) with a phonon frequency of 5.89 THz would require a temperature $T \gtrsim 6820$ K.

IV. CONCLUSION

Ab initio calculations demonstrate that the dynamical stabilization of cubic ZrO_2 is entropy driven and can be ascribed to the interaction between the X_2^- phonon and other phonons of the crystal. This contradicts the assumption that the phonons remain independent, which served to justify previous calculations that treated the unstable mode as an independent anharmonic oscillator. The dynamical stabilization of cubic zirconia by phonon-phonon interactions, as well as similar results for the bcc phase of Ti, Zr, and Hf, suggests that the same mechanism likely plays a key role in more systems than previously assumed. Therefore, the calculation of thermodynamic properties of such systems will require the inclusion of phonon-phonon interactions, which will be possible with the SCAILD method once further developments have been made to overcome the slow convergence with respect to supercell size.

Furthermore, as a result of the phonon-phonon interaction in cubic ZrO_2, the effective potential experienced by the X_2^- phonon mode at temperatures near 2570 K becomes quadratic. This quadratic form of the effective potential should influence the details of experimental measurements of cubic zirconia's lattice dynamics.

ACKNOWLEDGMENTS

The Department of Energy supported this work under Contract No. DE-AC52-06NA25396. We also want to acknowledge our appreciation to Alexander Mavromaras of Materials Design for suggesting cubic zirconia as an interesting material to study, and Olle Eriksson at Uppsala University for providing computer resources. We thank Eric Chisolm for helpful discussions.

[1] D. C. Wallace, *Statistical Physics of Crystals and Liquids* (World Scientific, New Jersey, 2002).
[2] K. Kunc and R. M. Martin, Phys. Rev. Lett. **48**, 406 (1982).
[3] P. Souvatzis, A. Delin, and O. Eriksson, Phys. Rev. B **73**, 054110 (2006).
[4] S. Baroni, P. Giannozzi, and A. Testa, Phys. Rev. Lett. **58**, 1861 (1987).
[5] S. Wei and M. Y. Chou, Phys. Rev. Lett. **69**, 2799 (1992).
[6] W. Frank, C. Elsasser, and M. Fahnle, Phys. Rev. Lett. **74**, 1791 (1995).
[7] K. Parlinski, Z-.Q. Li, and Y. Kawazoe, Phys. Rev. Lett. **78**, 4063 (1997).
[8] Sven P. Rudin, M. D. Jones, C. W. Greeff, and R. C. Albers, Phys. Rev. B **65**, 235114 (2002).
[9] V. L. Moruzzi, J. F. Janak, and K. Schwarz, Phys. Rev. B **37**, 790 (1988).
[10] P. Söderlind, L. Nordström, Lou Yongming, and B. Johansson, Phys. Rev. B **42**, 4544 (1990).
[11] M. Born and K. Huang, *Dynamical Theory of Crystal Lattices* (Oxford University Press, Oxford, 1954).
[12] Kristin Persson, Mathias Ekman, and Vidvuds Ozolins, Phys. Rev. B **61**, 11221 (2000).
[13] M. Sternik and K. Parlinski, J. Chem. Phys. **123**, 204708 (2005).
[14] A. B. Belonoshko, N. V. Skorodumova, A. Rosengren, and B. Johansson, Science **319**, 797 (2008).
[15] L. Vočadlo, D. Alfè, M. J. Gillan, I. G. Wood, J. P. Brodholt, and G. D. Price, Nature (London) **424**, 536 (2003).
[16] N. D. Drummond and G. J. Ackland, Phys. Rev. B **65**, 184104 (2002).
[17] M. B. Smirnov, Phys. Rev. B **59**, 4036 (1999).
[18] M. B. Smirnov and J. Hlinka, Phys. Solid State **42**, 064707 (2000).
[19] C. Zener, in *Influence of Entropy on Phase Stabilization in Phase Stability in Metals and Alloys*, edited by P. S. Rudman, J. Stringer, and R. I. Jaffee (McGraw-Hill, New York, 1967), p. 25.
[20] Y. Y. Ye, Y. Chen, K. M. Ho, B. N. Harmon, and P. A. Lindgård, Phys. Rev. Lett. **58**, 1769 (1987).
[21] A. Kuwabara, T. Tohei, T. Yamamoto, and I. Tanaka, Phys. Rev. B **71**, 064301 (2005).
[22] M. Sternik and K. Parlinski, J. Chem. Phys. **122**, 064707 (2005).
[23] P. Souvatzis, O. Eriksson, M. I. Katsnelson, and S. P. Rudin, Phys. Rev. Lett. **100**, 095901 (2008).
[24] P. Souvatzis, O. Eriksson, M. I. Katsnelson, and S. P. Rudin, Comput. Mater. Sci. (to be published).

[25] B. N. Harmon, W. Weber, and D. R. Hamann, Phys. Rev. B **25**, 1109 (1982).
[26] G. Kresse and J. Furthmuller, Phys. Rev. B **54**, 11169 (1996).
[27] J. P. Perdew and Y. Wang, Phys. Rev. B **45**, 13244 (1992).
[28] D. M. Ceperley and B. J. Alder, Phys. Rev. Lett. **45**, 566 (1980).
[29] E. V. Stefanovich, A. L. Shluger, and C. R. A. Catlow, Phys. Rev. B **49**, 11560 (1994).
[30] X. Gonze and C. Lee, Phys. Rev. B **55**, 10355 (1997).
[31] S. Baroni, S. de Gironcoli, A. Dal Corso, and P. Giannozzi, Rev. Mod. Phys. **73**, 515 (2001).